Measurement of the B^+ total cross section and B^+ differential cross section $d\sigma/dp_T$ in $p\bar{p}$ collisions at $\sqrt{s}=1.8$ TeV

D. Acosta,[13] T. Affolder,[24] H. Akimoto,[46] M. G. Albrow,[12] P. Amaral,[9] D. Ambrose,[33] D. Amidei,[26] K. Anikeev,[25] J. Antos,[1] G. Apollinari,[12] T. Arisawa,[46] A. Artikov,[10] T. Asakawa,[44] W. Ashmanskas,[9] F. Azfar,[31] P. Azzi-Bacchetta,[32] N. Bacchetta,[32] H. Bachacou,[24] S. Bailey,[17] P. de Barbaro,[37] A. Barbaro-Galtieri,[24] V. E. Barnes,[36] B. A. Barnett,[20] S. Baroiant,[5] M. Barone,[14] G. Bauer,[25] F. Bedeschi,[34] S. Belforte,[43] W. H. Bell,[16] G. Bellettini,[34] J. Bellinger,[47] D. Benjamin,[11] J. Bensinger,[4] A. Beretvas,[12] J. P. Berge,[12] J. Berryhill,[9] A. Bhatti,[38] M. Binkley,[12] D. Bisello,[32] M. Bishai,[12] R. E. Blair,[2] C. Blocker,[4] K. Bloom,[26] B. Blumenfeld,[20] S. R. Blusk,[37] A. Bocci,[38] A. Bodek,[37] G. Bolla,[36] Y. Bonushkin,[6] D. Bortoletto,[36] J. Boudreau,[35] A. Brandl,[28] S. van den Brink,[20] C. Bromberg,[27] M. Brozovic,[11] E. Brubaker,[24] N. Bruner,[28] E. Buckley-Geer,[12] J. Budagov,[10] H. S. Budd,[37] K. Burkett,[17] G. Busetto,[32] A. Byon-Wagner,[12] K. L. Byrum,[2] S. Cabrera,[11] P. Calafiura,[24] M. Campbell,[26] W. Carithers,[24] J. Carlson,[26] D. Carlsmith,[47] W. Caskey,[5] A. Castro,[3] D. Cauz,[43] A. Cerri,[34] A. W. Chan,[1] P. S. Chang,[1] P. T. Chang,[1] J. Chapman,[26] C. Chen,[33] Y. C. Chen,[1] M.-T. Cheng,[1] M. Chertok,[5] G. Chiarelli,[34] I. Chirikov-Zorin,[10] G. Chlachidze,[10] F. Chlebana,[12] L. Christofek,[19] M. L. Chu,[1] J. Y. Chung,[29] Y. S. Chung,[37] C. I. Ciobanu,[29] A. G. Clark,[15] A. P. Colijn,[12] A. Connolly,[24] M. Convery,[38] J. Conway,[39] M. Cordelli,[14] J. Cranshaw,[41] R. Culbertson,[12] D. Dagenhart,[45] S. D'Auria,[16] F. DeJongh,[12] S. Dell'Agnello,[14] M. Dell'Orso,[34] S. Demers,[37] L. Demortier,[38] M. Deninno,[3] P. F. Derwent,[12] T. Devlin,[39] J. R. Dittmann,[12] A. Dominguez,[24] S. Donati,[34] J. Done,[40] M. D'Onofrio,[34] T. Dorigo,[17] N. Eddy,[19] K. Einsweiler,[24] J. E. Elias,[12] E. Engels, Jr.,[35] R. Erbacher,[12] D. Errede,[19] S. Errede,[19] Q. Fan,[37] H.-C. Fang,[24] R. G. Feild,[48] J. P. Fernandez,[12] C. Ferretti,[34] R. D. Field,[13] I. Fiori,[3] B. Flaugher,[12] G. W. Foster,[12] M. Franklin,[17] J. Freeman,[12] J. Friedman,[25] Y. Fukui,[23] I. Furic,[25] S. Galeotti,[34] A. Gallas,[17,*] M. Gallinaro,[38] T. Gao,[33] M. Garcia-Sciveres,[24] A. F. Garfinkel,[36] P. Gatti,[32] C. Gay,[48] D. W. Gerdes,[26] E. Gerstein,[8] P. Giannetti,[34] P. Giromini,[14] V. Glagolev,[10] D. Glenzinski,[12] M. Gold,[28] J. Goldstein,[12] I. Gorelov,[28] A. T. Goshaw,[11] Y. Gotra,[35] K. Goulianos,[38] C. Green,[36] G. Grim,[5] P. Gris,[12] C. Grosso-Pilcher,[9] M. Guenther,[36] G. Guillian,[26] J. Guimaraes da Costa,[17] R. M. Haas,[13] C. Haber,[24] S. R. Hahn,[12] C. Hall,[17] T. Handa,[18] R. Handler,[47] W. Hao,[41] F. Happacher,[14] K. Hara,[44] A. D. Hardman,[36] R. M. Harris,[12] F. Hartmann,[21] K. Hatakeyama,[38] J. Hauser,[6] J. Heinrich,[33] A. Heiss,[21] M. Herndon,[20] C. Hill,[5] A. Hocker,[37] K. D. Hoffman,[9] R. Hollebeek,[33] L. Holloway,[19] B. T. Huffman,[31] R. Hughes,[29] J. Huston,[27] J. Huth,[17] H. Ikeda,[44] J. Incandela,[12,†] G. Introzzi,[34] A. Ivanov,[37] J. Iwai,[46] Y. Iwata,[18] E. James,[26] M. Jones,[33] U. Joshi,[12] H. Kambara,[15] T. Kamon,[40] T. Kaneko,[44] M. Karagoz Unel,[40,*] K. Karr,[45] S. Kartal,[12] H. Kasha,[48] Y. Kato,[30] T. A. Keaffaber,[36] K. Kelley,[25] M. Kelly,[26] D. Khazins,[11] T. Kikuchi,[44] B. Kilminster,[37] B. J. Kim,[22] D. H. Kim,[22] H. S. Kim,[19] M. J. Kim,[8] S. B. Kim,[22] S. H. Kim,[44] Y. K. Kim,[24] M. Kirby,[11] M. Kirk,[4] L. Kirsch,[4] S. Klimenko,[13] P. Koehn,[29] K. Kondo,[46] J. Konigsberg,[13] A. Korn,[25] A. Korytov,[13] E. Kovacs,[2] J. Kroll,[33] M. Kruse,[11] S. E. Kuhlmann,[2] K. Kurino,[18] T. Kuwabara,[44] A. T. Laasanen,[36] N. Lai,[9] S. Lami,[38] S. Lammel,[12] J. Lancaster,[11] M. Lancaster,[24] R. Lander,[5] A. Lath,[39] G. Latino,[34] T. LeCompte,[2] K. Lee,[41] S. Leone,[34] J. D. Lewis,[12] M. Lindgren,[6] T. M. Liss,[19] J. B. Liu,[37] Y. C. Liu,[1] D. O. Litvintsev,[12] O. Lobban,[41] N. S. Lockyer,[33] J. Loken,[31] M. Loreti,[32] D. Lucchesi,[32] P. Lukens,[12] S. Lusin,[47] L. Lyons,[31] J. Lys,[24] R. Madrak,[17] K. Maeshima,[12] P. Maksimovic,[17] L. Malferrari,[3] M. Mangano,[34] M. Mariotti,[32] G. Martignon,[32] A. Martin,[48] J. A. J. Matthews,[28] P. Mazzanti,[3] K. S. McFarland,[37] P. McIntyre,[40] M. Menguzzato,[32] A. Menzione,[34] P. Merkel,[12] C. Mesropian,[38] A. Meyer,[12] T. Miao,[12] R. Miller,[27] J. S. Miller,[26] H. Minato,[44] S. Miscetti,[14] M. Mishina,[23] G. Mitselmakher,[13] Y. Miyazaki,[30] N. Moggi,[3] E. Moore,[28] R. Moore,[26] Y. Morita,[23] T. Moulik,[36] M. Mulhearn,[25] A. Mukherjee,[12] T. Muller,[21] A. Munar,[34] P. Murat,[12] S. Murgia,[27] J. Nachtman,[6] V. Nagaslaev,[41] S. Nahn,[48] H. Nakada,[44] I. Nakano,[18] C. Nelson,[12] T. Nelson,[12] C. Neu,[29] D. Neuberger,[21] C. Newman-Holmes,[12] C.-Y. P. Ngan,[25] H. Niu,[4] L. Nodulman,[2] A. Nomerotski,[13] S. H. Oh,[11] Y. D. Oh,[22] T. Ohmoto,[18] T. Ohsugi,[18] R. Oishi,[44] T. Okusawa,[30] J. Olsen,[47] W. Orejudos,[24] C. Pagliarone,[34] F. Palmonari,[34] R. Paoletti,[34] V. Papadimitriou,[41] D. Partos,[4] J. Patrick,[12] G. Pauletta,[43] M. Paulini,[8] C. Paus,[25] D. Pellett,[5] L. Pescara,[32] T. J. Phillips,[11] G. Piacentino,[34] K. T. Pitts,[19] A. Pompos,[36] L. Pondrom,[47] G. Pope,[35] F. Prokoshin,[10] J. Proudfoot,[2] F. Ptohos,[14] O. Pukhov,[10] G. Punzi,[34] A. Rakitine,[25] F. Ratnikov,[39] D. Reher,[24] A. Reichold,[31] P. Renton,[31] A. Ribon,[32] W. Riegler,[17] F. Rimondi,[3] L. Ristori,[34] M. Riveline,[42] W. J. Robertson,[11] T. Rodrigo,[7] S. Rolli,[45] L. Rosenson,[25] R. Roser,[12] R. Rossin,[32] C. Rott,[36] A. Roy,[36] A. Ruiz,[7] A. Safonov,[5] R. St. Denis,[16] W. K. Sakumoto,[37] D. Saltzberg,[6] C. Sanchez,[29] A. Sansoni,[14] L. Santi,[43] H. Sato,[44] P. Savard,[42] A. Savoy-Navarro,[12] P. Schlabach,[12] E. E. Schmidt,[12] M. P. Schmidt,[48] M. Schmitt,[17,*] L. Scodellaro,[32] A. Scott,[6] A. Scribano,[34] A. Sedov,[36] S. Segler,[12] S. Seidel,[28] Y. Seiya,[44] A. Semenov,[10] F. Semeria,[3] T. Shah,[25] M. D. Shapiro,[24] P. F. Shepard,[35] T. Shibayama,[44] M. Shimojima,[44] M. Shochet,[9] A. Sidoti,[32] J. Siegrist,[24] A. Sill,[41] P. Sinervo,[42] P. Singh,[19] A. J. Slaughter,[48] K. Sliwa,[45] C. Smith,[20] F. D. Snider,[12] A. Solodsky,[38] J. Spalding,[12] T. Speer,[15] P. Sphicas,[25] F. Spinella,[34] M. Spiropulu,[9] L. Spiegel,[12] J. Steele,[47] A. Stefanini,[34] J. Strologas,[19] F. Strumia,[15] D. Stuart,[12] K. Sumorok,[25] T. Suzuki,[44] T. Takano,[30] R. Takashima,[18] K. Takikawa,[44] P. Tamburello,[11] M. Tanaka,[44] B. Tannenbaum,[6] M. Tecchio,[26] R. J. Tesarek,[12] P. K. Teng,[1] K. Terashi,[38] S. Tether,[25] A. S. Thompson,[16] E. Thomson,[29] R. Thurman-Keup,[2] P. Tipton,[37] S. Tkaczyk,[12] D. Toback,[40] K. Tollefson,[37] A. Tollestrup,[12] D. Tonelli,[34] H. Toyoda,[30] W. Trischuk,[42] J. F. de Troconiz,[17] J. Tseng,[25] D. Tsybychev,[13] N. Turini,[34] F. Ukegawa,[44] T. Vaiciulis,[37] J. Valls,[39] S. Vejcik III,[12] G. Velev,[12] G. Veramendi,[24] R. Vidal,[12] I. Vila,[7] R. Vilar,[7] I. Volobouev,[24] M. von der Mey,[6] D. Vucinic,[25] R. G. Wagner,[2] R. L. Wagner,[12] N. B. Wallace,[39] Z. Wan,[39]

C. Wang,[11] M. J. Wang,[1] S. M. Wang,[13] B. Ward,[16] S. Waschke,[16] T. Watanabe,[44] D. Waters,[31] T. Watts,[39] R. Webb,[40] H. Wenzel,[21] W. C. Wester III,[12] A. B. Wicklund,[2] E. Wicklund,[12] T. Wilkes,[5] H. H. Williams,[33] P. Wilson,[12] B. L. Winer,[29] D. Winn,[26] S. Wolbers,[12] D. Wolinski,[26] J. Wolinski,[27] S. Wolinski,[26] S. Worm,[39] X. Wu,[15] J. Wyss,[34] W. Yao,[24] G. P. Yeh,[12] P. Yeh,[1] J. Yoh,[12] C. Yosef,[27] T. Yoshida,[30] I. Yu,[22] S. Yu,[33] Z. Yu,[48] A. Zanetti,[43] F. Zetti,[24] and S. Zucchelli[3]

(CDF Collaboration)

[1]*Institute of Physics, Academia Sinica, Taipei, Taiwan 11529, Republic of China*
[2]*Argonne National Laboratory, Argonne, Illinois 60439*
[3]*Istituto Nazionale di Fisica Nucleare, University of Bologna, I-40127 Bologna, Italy*
[4]*Brandeis University, Waltham, Massachusetts 02254*
[5]*University of California at Davis, Davis, California 95616*
[6]*University of California at Los Angeles, Los Angeles, California 90024*
[7]*Instituto de Fisica de Cantabria, CSIC-University of Cantabria, 39005 Santander, Spain*
[8]*Carnegie Mellon University, Pittsburgh, Pennsylvania 15218*
[9]*Enrico Fermi Institute, University of Chicago, Chicago, Illinois 60637*
[10]*Joint Institute for Nuclear Research, RU-141980 Dubna, Russia*
[11]*Duke University, Durham, North Carolina 27708*
[12]*Fermi National Accelerator Laboratory, Batavia, Illinois 60510*
[13]*University of Florida, Gainesville, Florida 32611*
[14]*Laboratori Nazionali di Frascati, Istituto Nazionale di Fisica Nucleare, I-00044 Frascati, Italy*
[15]*University of Geneva, CH-1211 Geneva 4, Switzerland*
[16]*Glasgow University, Glasgow G12 8QQ, United Kingdom*
[17]*Harvard University, Cambridge, Massachusetts 02138*
[18]*Hiroshima University, Higashi-Hiroshima 724, Japan*
[19]*University of Illinois, Urbana, Illinois 61801*
[20]*The Johns Hopkins University, Baltimore, Maryland 21218*
[21]*Institut für Experimentelle Kernphysik, Universität Karlsruhe, 76128 Karlsruhe, Germany*
[22]*Center for High Energy Physics, Kyungpook National University, Taegu 702-701, Korea;*
Seoul National University, Seoul 151-742, Korea;
and SungKyunKwan University, Suwon 440-746, Korea
[23]*High Energy Accelerator Research Organization (KEK), Tsukuba, Ibaraki 305, Japan*
[24]*Ernest Orlando Lawrence Berkeley National Laboratory, Berkeley, California 94720*
[25]*Massachusetts Institute of Technology, Cambridge, Massachusetts 02139*
[26]*University of Michigan, Ann Arbor, Michigan 48109*
[27]*Michigan State University, East Lansing, Michigan 48824*
[28]*University of New Mexico, Albuquerque, New Mexico 87131*
[29]*The Ohio State University, Columbus, Ohio 43210*
[30]*Osaka City University, Osaka 588, Japan*
[31]*University of Oxford, Oxford OX1 3RH, United Kingdom*
[32]*Universita di Padova, Istituto Nazionale di Fisica Nucleare, Sezione di Padova, I-35131 Padova, Italy*
[33]*University of Pennsylvania, Philadelphia, Pennsylvania 19104*
[34]*Istituto Nazionale di Fisica Nucleare, University and Scuola Normale Superiore of Pisa, I-56100 Pisa, Italy*
[35]*University of Pittsburgh, Pittsburgh, Pennsylvania 15260*
[36]*Purdue University, West Lafayette, Indiana 47907*
[37]*University of Rochester, Rochester, New York 14627*
[38]*Rockefeller University, New York, New York 10021*
[39]*Rutgers University, Piscataway, New Jersey 08855*
[40]*Texas A&M University, College Station, Texas 77843*
[41]*Texas Tech University, Lubbock, Texas 79409*
[42]*Institute of Particle Physics, University of Toronto, Toronto M5S 1A7, Canada*
[43]*Istituto Nazionale di Fisica Nucleare, University of Trieste/Udine, Italy*
[44]*University of Tsukuba, Tsukuba, Ibaraki 305, Japan*
[45]*Tufts University, Medford, Massachusetts 02155*
[46]*Waseda University, Tokyo 169, Japan*
[47]*University of Wisconsin, Madison, Wisconsin 53706*
[48]*Yale University, New Haven, Connecticut 06520*

(Received 31 October 2001; published 5 February 2002)

We present measurements of the B^+ meson total cross section and differential cross section $d\sigma/dp_T$. The measurements use a 98 ± 4 pb^{-1} sample of $p\bar{p}$ collisions at $\sqrt{s}=1.8$ TeV collected by the CDF detector. Charged B meson candidates are reconstructed through the decay $B^\pm\to J/\psi K^\pm$ with $J/\psi\to\mu^+\mu^-$. The total cross section, measured in the central rapidity region $|y|<1.0$ for $p_T(B)>6.0$ GeV/c, is 3.6 ± 0.6(stat $\oplus$ syst) μb. The measured differential cross section is substantially larger than typical QCD predictions calculated to next-to-leading order.

DOI: 10.1103/PhysRevD.65.052005 PACS number(s): 13.85.Ni, 12.38.Qk, 13.25.Hw, 14.40.Nd

I. INTRODUCTION

Quantum chromodynamics (QCD) can be used to compute the expected cross sections for the production of heavy quarks at hadron collider energies. Calculations of the hard-scattering cross section have been carried out to next-to-leading order in perturbation theory [1]. Experimental measurements must show that these predictions provide an adequate description of the cross section at 1.8 TeV before they can be confidently extrapolated to higher energies or more exotic phenomena. Unfortunately the QCD predictions are affected by large theoretical uncertainties such as the dependence on the choice of the factorization and renormalization scales, the parton density parametrization and the b quark mass [2].

Experiments at CERN [3] and at the Fermilab Tevatron [4] have shown that the b quark production cross section is higher than the theoretical predictions obtained with the standard choice of parameters by about a factor of 2–3. Closer agreement between theory and the experimental measurements can be achieved by choosing rather extreme values of the theoretical parameters [2]. It has also been suggested that the large discrepancy could be explained by pair production of light gluinos that decay into bottom quarks and bottom squarks [5].

This paper describes a measurement of the B^+ meson total cross section and differential cross section $d\sigma/dp_T$ in hadronic collisions using fully reconstructed $B^\pm$ mesons decaying into the exclusive final state $J/\psi K^\pm$. The measurement uses a data sample of 98 ± 4 pb^{-1} collected by the Collider Detector at Fermilab (CDF) experiment from $p\bar{p}$ collisions with a center-of-mass energy of 1.8 TeV produced by the Fermilab Tevatron. The data were collected in the run period from 1992 to 1995 which is referred to as run 1. Our previously published result [6] based upon 19.3 ± 0.7 pb^{-1} of data (run 1A) found that the total cross section for $p_T(B)>6.0$ GeV/c and $|y|<1.0$ is $\sigma_B=2.39\pm0.54$(stat $\oplus$ syst) μb.

The paper is organized as follows. In Sec. II we review previous measurements of the B cross section using exclusive B decays. In Sec. III we briefly describe the components of the CDF detector relevant to the analysis presented in this paper. The data collection, event selection procedures and the reconstruction of $B^\pm\to J/\psi K^\pm$ are discussed in Sec. IV. The measurement of the differential and total cross sections is presented in Secs. V and VI, respectively.

II. PREVIOUS MEASUREMENT OF THE B PRODUCTION CROSS SECTION

The run 1A measurement of the B meson differential cross section was determined from fully reconstructing the decays $B^\pm\to J/\psi K^\pm$ and $B^0\to J/\psi K^*(892)^0$ [6]. The measurement of the B transverse momentum spectrum showed that next-to-leading-order QCD adequately described the shape of this distribution for $p_T>6.0$ GeV/c. In the run 1A publication, CDF used a branching ratio $BR(B^+\to J/\psi K^+)=(11.0\pm1.7)\times10^{-4}$ and a product of branching fractions $\mathcal{B}=BR(B^+\to J/\psi K^+)\times BR(J/\psi\to\mu^+\mu^-)=(6.55\pm1.01)\times10^{-5}$ [7]. The current world average for $BR(B^+\to J/\psi K^+)$ is $(10.0\pm1.0)\times10^{-4}$ which yields $\mathcal{B}=(5.88\pm0.60)\times10^{-5}$. The change in the branching fractions scales the published result up by about 10% to $\sigma_B(p_T>6.0$ GeV/$c,|y|<1.0)=2.66\pm0.61$ (stat $\oplus$ syst)μb.

This paper updates the measurement presented in 1995 by using the complete run 1 data sample of 98 ± 4 pb^{-1}. For this measurement, we use only the decay mode $B^\pm\to J/\psi K^\pm$ where we require both muon candidates from the J/ψ decay to be well measured by the silicon vertex detector (SVX). Such a restriction allows us to use fewer selection requirements since the decay mode $B^\pm\to J/\psi K^\pm$ has a lower combinatorial background than $B^0\to J/\psi K^{*0}$, and the SVX information enables us to substantially reduce the prompt background. Moreover, several of the efficiencies are measured using a large sample of $J/\psi\to\mu^+\mu^-$ candidates rather than relying on Monte Carlo calculations for detailed modeling of detector effects.

III. THE CDF DETECTOR

The CDF detector is described in detail in [8]. We summarize here the features of the detector subsystems that are important for this analysis. The CDF coordinate system has the z axis pointing along the proton beam momentum, and the angle ϕ is measured from the plane of the Tevatron storage ring. The transverse (r-ϕ) plane is normal to the proton beam.

The CDF experiment uses three separate detectors for tracking charged particles: the silicon vertex detector (SVX), the vertex detector (VTX), and the central tracking chamber (CTC). These devices are immersed in a magnetic field of 1.4 Tesla pointed along the $-z$ axis generated by a superconducting solenoid of length 4.8 m and radius 1.5 m.

The innermost device is the SVX [9] which provides spa-

*Present address: Northwestern University, Evanston, IL 60208.
†Present address: University of California, Santa Barbara, CA 93106.

tial measurements in the r-ϕ plane. The SVX consists of two cylindrical barrels that cover a region 51 cm long in z. Each barrel consists of four layers of silicon strip sensors with strips oriented parallel to the beam axis. The distribution of the $p\bar{p}$ collisions along the beamline is Gaussian in z with a σ of about 30 cm. Therefore only about 60% of all $J/\psi \rightarrow \mu^+\mu^-$ events have both muon tracks reconstructed in the SVX.

The SVX is surrounded by the VTX, a set of time projection chambers which measure the z coordinate of the $p\bar{p}$ interaction (primary vertex). Surrounding the SVX and the VTX is the CTC. The CTC is a 3.2 m long cylindrical drift chamber with 84 layers of sense wires ranging in radius from 31 cm to 133 cm. The combined momentum resolution of the tracking chambers is $\delta p_T/p_T=[(0.0009p_T)^2+(0.0066)^2]^{1/2}$ where p_T is the component of the momentum transverse to the z axis and is measured in GeV/c. Charged track trajectories reconstructed in the CTC that are matched to strip clusters in the SVX have an impact parameter resolution of $\sigma_d(p_T)=(13+40/p_T)$ μm [10] with p_T in units of GeV/c. The track impact parameter d is defined as the distance of closest approach of the track helix to the beam axis measured in the plane perpendicular to the beam.

The central muon system consists of three components (CMU, CMP and CMX) and detects muons with $p_T \geq 1.4$ GeV/c in the pseudorapidity range $|\eta|<1.0$. The CMU system covers the region $|\eta|<0.6$ and consists of four layers of drift chambers outside the hadron calorimeter. Outside the CMU there is an additional absorber of 60 cm of steel followed by four layers of drift chambers (CMP). The CMX system extends the coverage to pseudorapidity $0.6<|\eta|<1.0$ but is not used in this analysis.

CDF employs a three level trigger system. The first two levels are implemented in custom electronics. To select events in the third level, we employ a CPU farm using a version of the CDF event reconstruction program optimized for speed.

IV. DATA SAMPLE SELECTION

A. Dimuon trigger

The data sample consists of events that pass the $J/\psi \rightarrow \mu^+\mu^-$ trigger. In the first level of this trigger, we require two muon track segments in the central muon chambers separated by at least 5° in azimuth. The trigger efficiency for each muon at level 1 rises from 50% for $p_T=1.7$ GeV/c to 95% for $p_T=3.3$ GeV/c.

In the second level, we require muon segments found in level 1 to be associated with tracks identified by the central fast tracker (CFT) [11]. The resolution of the CFT is $\delta p_T/p_T^2 \approx 0.03$ $(\mathrm{GeV}/c)^{-1}$. In run 1A and for a subset of the run 1B data, we required one of the two muons to be matched to a CFT track with p_T greater than about 3 GeV/c while in the bulk of the run 1B sample, we required two muon segments to have an associated track with a threshold of about 2 GeV/c. In run 1A (1B), the extrapolation of the track was required to be typically within 10° (5°) of the muon segment. The efficiency of the track requirements was measured in a J/ψ data sample using events in which the muon under study need not have satisfied the requirements for the event to be accepted. The efficiency for the nominal 2 (3) GeV/c threshold rose from 50% of the plateau efficiency at 1.95 (3.05) GeV/c to 95% of the plateau efficiency at 2.2 (3.4) GeV/c. That plateau efficiency changed over the course of the run because of aging of the CTC and subsequent modifications to the CFT algorithms. That dependence on time is accounted for in the calculation of the trigger efficiencies.

The level 3 software trigger required two muon candidates with an effective mass in the J/ψ mass region after full reconstruction. Runs with known hardware problems for muons were removed yielding for this analysis a total run 1 luminosity of 98 pb^{-1}.

B. J/ψ reconstruction

Background events in the dimuon sample collected with these triggers are suppressed by applying additional muon selection cuts. Track quality requirements are used to reduce the backgrounds arising from poor track measurements. Tighter cuts are imposed on the correlation between the track in the muon chamber and the extrapolated CTC track.

The transverse momentum of each muon from the J/ψ for run 1A is required to be greater than 1.8 GeV/c with one muon of the pair greater than 2.8 GeV/c. For run 1B, both muons are required to have a transverse momentum greater than 2.0 GeV/c. Events passing both the trigger and p_T requirements identical to those of run 1A are also accepted. The muons must have opposite charge and the separation in z between the two tracks must be less than 5.0 cm at the point of closest approach to the beamline. The z coordinate of the decay vertex is required to be within ± 60 cm of the detector center.

The invariant mass and uncertainty (σ_m) of the J/ψ candidates are calculated after constraining the two muon tracks to come from a common point in space (vertex constraint) to improve the mass resolution. The width of the reconstructed J/ψ mass peak is 16 MeV/c^2. The signal region is defined to be those dimuon candidates with reconstructed mass within $3.3\sigma_m$ of the known J/ψ mass [12]. We find $(8.7 \pm 0.2)\times 10^4$ J/ψ over background. In this analysis, the two muons from the J/ψ decay are required to be reconstructed in the silicon detector.

C. Primary vertex selection

Knowledge of the distance between the primary $p\bar{p}$ interaction vertex and the secondary decay vertex in the transverse plane is crucial to this analysis since the B meson proper lifetime is used to discriminate between B mesons and background events. We find the transverse position of the primary vertex using the average beamline calculated for each Tevatron $p\bar{p}$ store [13]. The longitudinal coordinate of the primary vertex (z) is measured using data from the VTX detector. The slopes and intercepts of the run-averaged beam position are combined with the event-by-event z locations of

the vertices to determine the vertex position. The primary vertex uncertainties σ_x, σ_y and σ_z are estimated to be 25, 25 and 300 μm, respectively.

D. *B* reconstruction

To select charged B candidates we considered each charged particle track as a kaon candidate to be combined with a J/ψ. A charged track in an event is combined with the two muons if the z_0 parameter of the track is within 5 cm of the z position of the J/ψ candidate decay vertex. The exit radius of the kaon candidate, which corresponds to the radius at which the track trajectory intersects the plane of the CTC endplate, is required to be greater than 110 cm to limit the search to a region of high tracking efficiency. A cut on the kaon transverse momentum of $p_T > 1.25$ GeV/c is imposed to reduce the large combinatorial background. This cut is very effective since kaons from B meson decay have a considerably harder p_T spectrum than particles from the underlying event and from events with prompt J/ψ production. The muon and kaon tracks are constrained to come from a common point of origin and the mass of the $\mu^+\mu^-$ pair is constrained to the known J/ψ mass. Since the intrinsic width of the J/ψ is significantly smaller than our experimental resolution, the mass constraint improves the resolution of the reconstructed B mass.

The p_T of each B candidate is required to be greater than 6.0 GeV/c. The proper decay length is required to be greater than 100 μm to suppress backgrounds associated with prompt J/ψ mesons. The signed proper decay length in the B rest frame is defined as

$$ct(B) = \frac{\overrightarrow{X_{J/\psi}} \cdot \overrightarrow{p_T^B}}{p_T^B} \cdot \frac{1}{(\beta\gamma)^B} = \frac{M_B \overrightarrow{X_{J/\psi}} \cdot \overrightarrow{p_T^B}}{(p_T^B)^2} \tag{1}$$

where

$$\overrightarrow{X_{J/\psi}} = (x_{J/\psi} - x_{PV})\hat{i} + (y_{J/\psi} - y_{PV})\hat{j} \tag{2}$$

and $(\beta\gamma)^B$ is the relativistic boost of the B meson. The $(x_{J/\psi}, y_{J/\psi})$ are the transverse coordinates of the J/ψ decay vertex, and the (x_{PV}, y_{PV}) are the transverse coordinates of the event primary vertex. The intersection of the muon tracks as measured in the SVX determines the location of the B meson decay.

The $B^\pm$ candidate mass distribution is shown in Fig. 1. The distribution is fit with a Gaussian signal function plus a linear background using an unbinned maximum likelihood fit. The region below 5.15 GeV/c^2 has been excluded from the fit since it includes contributions from partially reconstructed higher-multiplicity B-decay modes. The fit yields 387 ± 32 $B^\pm$ mesons.

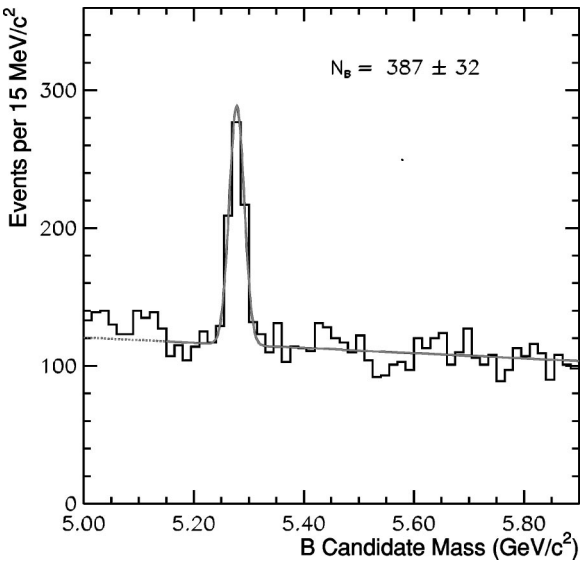

FIG. 1. $B^\pm$ invariant mass distribution reconstructed from the decay $B^\pm \to J/\psi K^\pm$. The curve is a binned fit to a Gaussian distribution plus linear background and is for illustration only.

V. DIFFERENTIAL CROSS SECTION

To measure the differential cross section, we divide the B candidate sample into four p_T ranges. The invariant mass distributions for each of the p_T ranges are then fitted using an unbinned maximum likelihood fit which is described in Sec. V A. The determination of the geometric acceptance, the efficiencies and the luminosity are described in Secs. V B, V C and V D respectively. The systematic uncertainties are discussed in Sec. V E, and the results are presented in Sec. V F.

A. Fitting technique

To measure the B^+ meson differential cross section as a function of p_T, the B candidate sample is divided into four p_T bins: 6–9, 9–12, 12–15, and 15–25 GeV/c. The invariant mass distribution for each of the p_T ranges is then fitted using an unbinned maximum likelihood fit to determine the number of B candidates in each p_T range, as shown in Fig. 2. The likelihood function is a Gaussian signal plus a linear background:

$$\mathcal{L} = \frac{N_{sig}}{N_{total}} f_{sig} + \frac{(N_{total} - N_{sig})}{N_{total}} f_{back} \tag{3}$$

where the free parameter N_{sig} is the number of signal events and N_{total} is the total number of candidates in each momentum bin. The function f_{sig} is the Gaussian signal mass function:

$$f_{sig} = \frac{1}{\sqrt{2\pi} s \sigma_i} e^{-1/2[(M_i - M)/s\sigma_i]^2} \tag{4}$$

where M_i is the candidate mass obtained from a kinematic fit of the muon and kaon tracks. The uncertainty σ_i on the mass is scaled by a free parameter s in the unbinned maximum likelihood fit which is typically ≈ 1.2. The parameter M is the mean B mass obtained by fitting Fig. 1. The background mass function is linear:

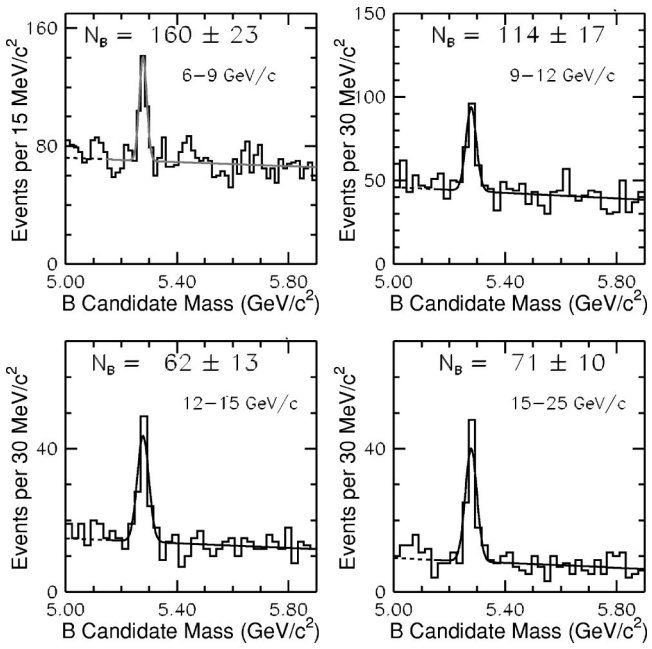

FIG. 2. $B^{\pm}$ candidate mass distribution for the four p_T ranges. The curve is a binned fit to a Gaussian distribution plus linear background and is for illustration only.

$$f_{back} = b\left(M_i - \frac{w}{2}\right) + \frac{1}{w} \tag{5}$$

where b is the slope of the background and w is the mass range in the fit (5.15 to 6.0 GeV/c^2). The region well above the B mass yields a better estimate of the slope of the background since it is not affected by partially reconstructed B decays. The likelihood function is minimized with respect to the parameters N_{sig}, s and b. The fit yields 160 ± 23, 114 ± 17, 62 ± 13 and 71 ± 10 events in the four transverse momentum bins.

B. Acceptances and trigger efficiencies

The acceptance is determined from a Monte Carlo simulation based on a next-to-leading-order QCD calculation [1] using the Martin-Roberts-Stirling-Thorne (MRST) parton distribution functions [14]. The b-quark pole mass m_b is taken to be 4.75 GeV/c^2. The b quarks are produced in the rapidity range $|y_b| < 1.1$ with $p_T(b) > 5.5$ GeV/c. The renormalization scale is $\mu = \mu_0 \equiv \sqrt{m_b^2 + p_T^2(b)}$, and the fragmentation scale is equal to the renormalization scale. The fragmentation into B mesons is modeled using the Peterson fragmentation function [15] with the parameter ϵ_P set to 0.006 [16]. This value was extracted in a fit to data collected at e^+e^- colliders. Recent results from the CERN e^+e^- collider LEP and SLAC Large Detector (SLD) suggest that lower values of ϵ_P and other functions better describe the fragmentation of b quarks into B hadrons [17]. Furthermore the assumption that a fragmentation function extracted from e^+e^- data is an accurate description of b fragmentation at a $p\bar{p}$ collider lacks a strong theoretical basis [2]. However, the uncertainties due to these factors are expected to be smaller than the uncertainty on the renormalization scale.

TABLE I. The product of the trigger efficiency and the acceptance in the p_T bins for run 1A, run 1B and the integrated luminosity-weighted average for run 1.

p_T range (GeV/c)	Trigger efficiency × acceptance (%) run 1A	run 1B	run 1
6–9	2.01 ± 0.02	1.61 ± 0.02	1.70 ± 0.02
9–12	5.29 ± 0.05	4.20 ± 0.04	4.44 ± 0.03
12–15	8.36 ± 0.10	6.53 ± 0.09	6.93 ± 0.07
15–25	11.96 ± 0.14	9.26 ± 0.12	9.86 ± 0.10

Decays of Monte Carlo–generated B mesons into the J/ψ and kaon final states are performed using a modified version of the CLEO Monte Carlo program [18] which accounts for the expected J/ψ longitudinal polarization. Once the B mesons are generated and decayed into their final state, a simulation of the CDF detector is utilized. A simulation of the trigger efficiency has also been included in the acceptance calculation. The events are then processed by the same analysis code used on the data to determine the combined acceptance and trigger efficiency for each momentum bin. The run 1A and 1B results which incorporate different trigger requirements are listed in Table I together with the combined results. The uncertainties given are statistical only.

C. Efficiencies of the additional selection requirements

The detector acceptance and trigger efficiencies described in the previous section did not account for all of the criteria for selecting a B candidate. The efficiencies of the additional selection requirements are discussed in this section. Most of these efficiencies are determined using large CDF data samples.

There are two components that comprise the tracking efficiencies. The first part is the efficiency of the tracking in the level 3 trigger system which is determined using an inclusive single muon data set. The efficiency is measured to be $(97 \pm 2)\%$ for run 1B. During run 1A, a portion of the data-taking suffered from the start time of each event being incorrectly determined. The result was an inefficiency in reconstruction at level 3 which was determined to be $\sim 4\%$ [19] averaged over all of run 1A. The level 3 run 1A efficiency is $(93 \pm 2)\%$.

Once an event has been accepted at level 3, one must account for the offline CTC track reconstruction which may improve the muon track quality or find new tracks that are missed at level 3. It is also necessary to correct for the track finding efficiency for the kaon track since it is not required in the level 3 trigger. A detailed study [20] of the CTC track reconstruction efficiencies was conducted. To measure the efficiency, we simulate single kaon tracks with the CDF Monte Carlo program. We then combine the generated CTC hits for such a kaon with the hits in an event with an identified displaced J/ψ from the CDF data sample. Hits in the CTC are characterized by a leading edge and a time-over-threshold. Where a real and simulated hit overlap, the hits are

TABLE II. Summary of reconstruction efficiencies for the B meson. The efficiencies that are not common between 1A and 1B are averaged and weighted by integrated luminosity.

Source	Efficiency in % Run 1A	Run 1B
CTC tracking	$(98.5\pm1.4)^3$ $=95.6\pm2.4$	$(99.6^{+0.4}_{-0.9})^3$ $=98.8^{+0.7}_{-1.5}$
L3 $\mu^+\mu^-$ tracking	93 ± 2	97 ± 2
CTC-μ linking	$(99.8\pm0.2)^2$ $=99.6\pm0.3$	
Muon chamber efficiency	$(98.0\pm1.0)^2$ $=96.0\pm1.4$	
$\mu^+\mu^-$ matching cut	98.7 ± 0.2	
Z vertex cut	95.3 ± 1.1	93.7 ± 1.1
SVX fraction	52.4 ± 0.6	56.3 ± 0.2
$ct>100$ μm	78.4 ± 0.5	
Total	36.4 ± 1.2	

combined. Thus the leading edges used in the track reconstruction may be obscured for the simulated kaon as they would be for real particles. We then run the full track reconstruction program on the modified event and search for a track corresponding to the embedded kaon. We find the efficiency of the track reconstruction to be $(99.6^{+0.4}_{-0.9})\%$ for particles with $p_T>0.8$ GeV/c that traversed all layers of the CTC, independent of instantaneous luminosity. The run 1A single track reconstruction efficiency of $(98.5\pm1.4)\%$ is taken from Ref. [6].

The muon segment reconstruction efficiency is found to be $(98.0\pm1.0)\%$ resulting in a combined efficiency of $(96.0\pm1.4)\%$. The efficiency of requiring both muons from the J/ψ to have a muon chamber track segment that matches a track reconstructed in the CTC is found to be $(98.7\pm0.2)\%$. The efficiency of this cut is determined from a sample of J/ψ candidate events containing muons that were required to pass less stringent matching requirements at level 3.

The fraction of events in which both muons from the J/ψ have been reconstructed in the SVX is measured using a large J/ψ data set. This fraction is $(52.4\pm0.6)\%$ for run 1A and $(56.3\pm0.2)\%$ for run 1B. The fraction for run 1B is larger than run 1A because the inner layer of the SVX detector was moved closer to the beamline, eliminating a small separation between silicon wafers in the first layer present in run 1A.

The efficiency to reconstruct a B meson with a proper decay length ct greater than 100 μm is determined using Monte Carlo simulations. The ct resolution is measured in the J/ψ data set by fitting the proper lifetime of events in the sidebands of the B candidate mass distribution with a Gaussian function for the prompt component and an exponential function for the long-lived component. The lifetimes of the Monte Carlo generated events are then smeared using the resolution measured in each p_T range. The efficiency showed no significant variation with the B transverse momentum even though the proper ct resolution was degraded by a factor of 2 from the lowest to the highest p_T bin. The efficiency of $(78.4\pm0.5)\%$ is the mean of the values measured in each p_T bin.

The reconstruction efficiencies are summarized in Table II. For the B candidates decaying to particles completely contained within the detector acceptance, the reconstruction efficiency is $(36.4\pm1.2)\%$.

D. Luminosity determination

At CDF the luminosity is measured using two telescopes of beam-beam counters to an accuracy of about 4%. We studied the quality of the integrated luminosity calculation in the inclusive $J/\psi\rightarrow\mu^+\mu^-$ sample. After correcting for the time-dependent trigger efficiency, we found that in run 1B the measured J/ψ cross section σ_ψ fell linearly as a function of instantaneous luminosity $\mathcal{L}$ [21]. However, for any narrow range of $\mathcal{L}$, σ_ψ was constant as a function of time. Since the minimum luminosity of the data sample is 4×10^{30} cm^{-2} s^{-1}, we have considered two possible extrapolations of σ_ψ as a function of $\mathcal{L}$ to $\mathcal{L}=0$ to calculate a corrected integrated luminosity. The first extrapolation is performed assuming that the linear dependence is valid below $\mathcal{L}<4\times10^{30}$ and that

$$\int \mathcal{L}'dt=\int \mathcal{L}(t)\frac{\sigma_\psi(0)}{\sigma_\psi(\mathcal{L})}dt. \tag{6}$$

We also perform the extrapolation assuming that no correction is needed below $\mathcal{L}<4\times10^{30}$. The luminosity correction is taken to be the average of the two extrapolations and we assign a systematic uncertainty that covers the range between the two hypotheses. The correction to the integrated luminosity for run 1B is

$$R_{\mathcal{L}}\equiv\int \mathcal{L}dt \Big/ \int \mathcal{L}'dt=0.88\pm0.04. \tag{7}$$

TABLE III. Summary of p_T dependent systematic uncertainties.

Source	Fractional uncertainty in each p_T bin			
p_T range (GeV/c)	6–9	9–12	12–15	15–25
QCD renormalization uncertainty	1.6%	1.5%	1.7%	1.5%
Peterson parameter uncertainty	0.7%	1.6%	1.0%	1.7%
Trigger efficiency uncertainty	3.1%	2.7%	2.1%	1.7%
p_T dependent total (syst$_{p_T}$)	3.6%	3.5%	2.9%	2.8%

TABLE IV. Summary of fully correlated systematic uncertainties.

Source	Fractional uncertainty
Reconstruction efficiency	$\pm 2.7\%$
Luminosity uncertainty	$\pm 4.1\%$
Luminosity correction	$\pm 4.5\%$
Branching ratio uncertainty	$\pm 10.2\%$
Kaon decay-in-flight uncertainty	$\pm 4.0\%$
Fully correlated total (syst_{fc})	$\pm 12.8\%$

E. Systematic uncertainties

We divide the systematic uncertainties in the measurement of the B^+ meson production cross section into two classes: p_T dependent uncertainties ($syst_{p_T}$) that change from one p_T bin to the next and fully correlated uncertainties ($syst_{fc}$) that are independent of p_T.

1. p_T dependent systematic uncertainties

The p_T dependent systematic uncertainties include variations of the production and decay kinematics that would affect the determination of the acceptance. We have considered effects due to the model used to generate the b quark spectrum and uncertainties in our knowledge of the trigger efficiency.

The model used to generate the b quarks is based on a QCD calculation at next-to-leading order. Large uncertainties in the calculation are due to unknown higher-order effects. These effects are quantified by estimating the scale dependence when the renormalization and factorization scales are varied by a factor of 2 above and below their central value of $\mu=\mu_0=\sqrt{p_T^2+m_b^2}$. The Peterson fragmentation parameter is varied by ± 0.002 around its central value of $\epsilon_P=0.006$. In each case the uncertainty on the acceptance is taken to be the difference between the acceptance found with the central value and the value found when each variable is varied by the indicated amounts. The dependence of acceptance on the parton density parametrization and the b quark mass are much smaller and are not included in the systematic uncertainty. In addition, the parameters of the trigger simulation are varied by $\pm 1\sigma$. The total p_T dependent uncertainty is given by the sum in quadrature of the p_T dependent systematic uncertainties summarized in Table III.

2. Correlated systematic uncertainties

The correlated systematic uncertainties include uncertainties that are independent of the B meson p_T spectrum. The largest of these uncertainties is due to limited knowledge of the $B^+\to J/\psi K^+$ branching ratio [12] which yields a systematic uncertainty of about 10%. Other sources of correlated uncertainties are due to the uncertainty on the total reconstruction efficiency shown in Table II and knowledge of the integrated luminosity collected at CDF during run 1. There is an additional systematic uncertainty associated with the reconstruction of kaons that decay inside the CTC volume. A simulation shows that about 8% of the kaons decay in flight, of which half are successfully reconstructed [6]. We assign the full value of the correction as an uncertainty for the kaon acceptance of $(96\pm 4)\%$. This assumes that such tracks are modeled realistically in the simulation. The total correlated uncertainty of 12.78% is given by the sum in quadrature of the fully correlated systematic uncertainties summarized in Table IV.

F. Results

The differential cross section $d\sigma/dp_T$ is calculated using the following equation:

$$\frac{d\sigma(B^+)}{dp_T}=\frac{N_{sig}/2}{\Delta p_T\cdot\mathcal{L}'\cdot A\cdot\epsilon\cdot\mathcal{B}} \tag{8}$$

where N_{sig} is the number of charged B mesons determined from the likelihood fit of the mass distribution in each p_T range. The factor of 1/2 is included because both B^+ and B^- mesons are detected while we report the cross section for B^+ mesons assuming charge invariance in the production process. The width of the p_T bin is Δp_T and $\mathcal{L}'$ is the corrected integrated luminosity of the sample. The geometric and kinematic acceptance A is determined from the Monte Carlo simulation and includes the kinematic and trigger efficiencies. The efficiency ϵ is the additional reconstruction efficiency not included in the simulation. The product of branching ratios $\mathcal{B}$ is determined using the the world-average [12] branching fractions:

$$BR(B^\pm\to J/\psi\ K^\pm)=(10.0\pm 1.0)\times 10^{-4} \tag{9}$$

$$BR(J/\psi\to\mu^+\mu^-)=(5.88\pm 0.10)\times 10^{-2}. \tag{10}$$

Table V lists the differential cross section as a function of p_T. The three uncertainties quoted on the cross section are statistical (stat), p_T dependent systematic (syst_{p_T}), and fully correlated systematic (syst_{fc}), respectively.

Figure 3 shows the measured differential cross section at the mean p_T of each bin compared to the next-to-leading-

TABLE V. B^+ meson differential cross section from the run 1 data.

$\langle p_T\rangle$ (GeV/c)	Events	Acceptance (%)	Cross section (nb/[GeV/c])
7.34	160 ± 23	1.70 ± 0.02	$815\pm 117(\text{stat})\pm 31(\text{syst}_{p_T})\pm 104(\text{syst}_{fc})$
10.35	114 ± 17	4.44 ± 0.03	$222\pm 33(\text{stat})\pm 8(\text{syst}_{p_T})\pm 28(\text{syst}_{fc})$
13.36	62 ± 13	6.93 ± 0.07	$77.5\pm 16.2(\text{stat})\pm 2.4(\text{syst}_{p_T})\pm 9.9(\text{syst}_{fc})$
18.87	71 ± 10	9.86 ± 0.10	$18.7\pm 2.6(\text{stat})\pm 0.6(\text{syst}_{p_T})\pm 2.4(\text{syst}_{fc})$

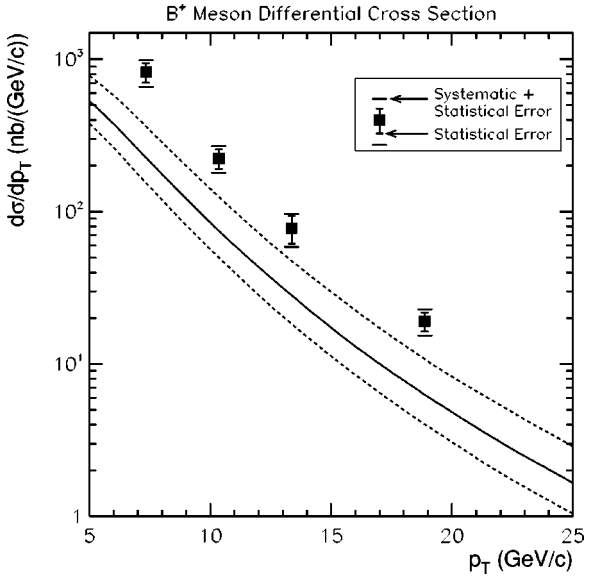

FIG. 3. B^+ meson differential cross measurements compared to the theoretical prediction. The solid curve is the theoretical prediction for $m_b=4.75$ GeV/c^2, $\mu_0=\sqrt{m_b^2+p_T^2}$, $\epsilon_P=0.006$ and $f_u=0.375$. The dashed lines illustrate the changes in the theory once these parameters are varied as explained in the text.

order QCD [1] calculation using the MRST parton density functions [14]. The experimental points are plotted at $\langle p_T\rangle$ which is the value of p_T for which the theoretical differential cross section [14] equals the mean cross section in each momentum range

$$\left.\frac{d\sigma}{dp_T}\right|_{\langle p_T\rangle}=\frac{1}{\Delta p_T}\int^{\Delta p_T}\frac{d\sigma}{dp_T}dp_T. \tag{11}$$

The dashed lines in Fig. 3 indicate the change in the theoretical predictions as the b quark mass is varied between 4.5 and 5.0 GeV/c^2, the renormalization scale is varied between $\mu_0/2$ and $2\mu_0$, and the Peterson fragmentation parameter is varied between 0.004 and 0.008. The solid curve is for the central values of these parameters: $m_b=4.75$ GeV/c^2, $\mu_0=\sqrt{m_b^2+p_T^2}$, and $\epsilon_P=0.006$. The fraction of $\bar{b}$ quarks that fragment into B^+ is $f_u=0.375\pm0.023$ [22]. This fraction is varied between 0.352 and 0.398.

The comparison between data and theory for $d\sigma/dp_T$ is aided by plotting the ratio of data/theory on a linear scale, as shown in Fig. 4. The level of agreement between the data and the theoretical prediction is determined by fitting a line through the four ratio points. The fit yields a scale factor for data/theory of 2.9 ± 0.2 $(\mathrm{stat}\oplus\mathrm{syst}_{p_T})\pm0.4$ (syst_{fc}) with a confidence level of 72%. The first uncertainty on the scale factor is the uncertainty returned by the fit to the ratio points whose uncertainties were determined by summing the statistical and the p_T dependent systematic uncertainties in quadrature. The second uncertainty is the fully correlated systematic uncertainty. The hatched band shows the magnitude of the fully correlated uncertainty which arises mainly due to the poor knowledge of the $B^+\to J/\psi K^+$ branching fraction. Also shown is a comparison between the shape of

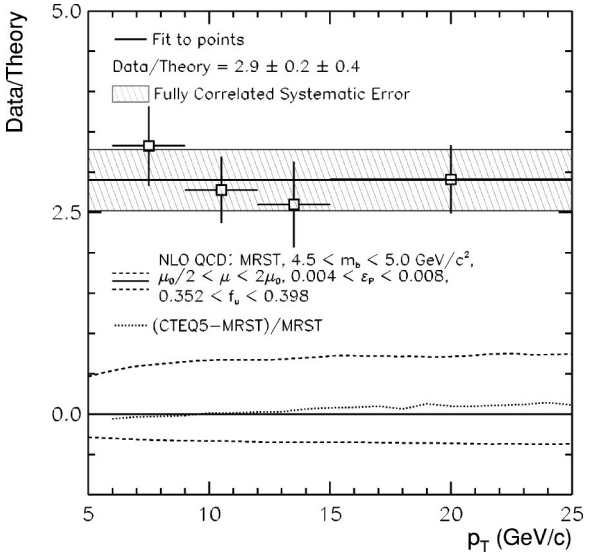

FIG. 4. Plot of data/theory as a shape comparison with the NLO QCD differential cross section calculations.

the QCD predictions obtained using a different set of parton distribution functions determined by the CTEQ Collaboration [23]. The effect of changing the parton distribution functions is negligible in comparison with the variation associated with uncertainties in the b quark mass, the fragmentation parameter and the renormalization scale shown by the dashed curves.

VI. THE TOTAL CROSS SECTION

The total cross section is obtained by using a method similar to the one used for the determination of the differential cross section. However, the last tranverse momentum bin, 15–25 GeV/c, is replaced with the invariant mass distribution for $B^\pm$ candidate events with $p_T>15$ GeV/c

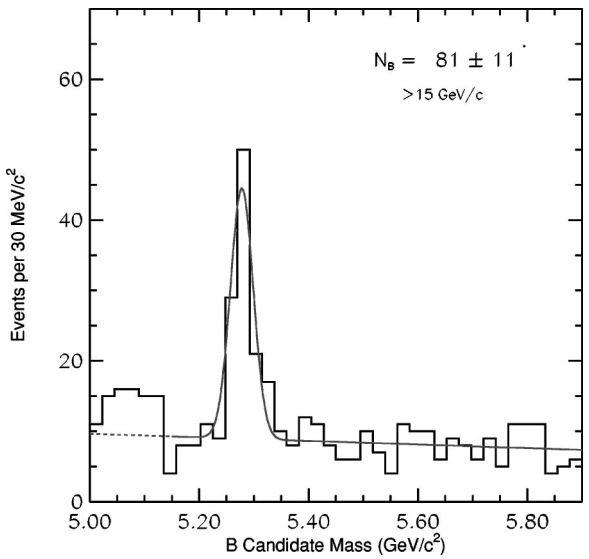

FIG. 5. $B^\pm$ candidate mass distribution for $p_T(B)>15$ GeV/c. The curve is a binned fit to a Gaussian distribution plus linear background and is for illustration only.

shown in Fig. 5. With 81 ± 11 candidates and an acceptance of $(10.19 \pm 0.16)\%$, the integrated cross section for $p_T > 15$ GeV/c is $207 \pm 28(\text{stat}) \pm 5(\text{syst}_{p_T}) \pm 26(\text{syst}_{fc})$ nb. The integrated cross section for B transverse momentum $p_T > 6.0$ GeV/c and $|y| < 1.0$ is given by:

$$\sigma(B^+) = \sum_{i=1}^{4} \frac{N_i/2}{\mathcal{L}' \cdot A_i \cdot \epsilon \cdot \mathcal{B}} \tag{12}$$

where N_i is the number of charged B candidate events in each momentum bin, A_i is the acceptance and ϵ is reconstruction efficiency. The total cross section is:

$$\sigma_B(p_T > 6.0 \text{ GeV}/c, |y| < 1.0) = 3.6 \pm 0.4 \ (\text{stat} \oplus \text{syst}_{p_T}) \pm 0.4 \ (\text{syst}_{fc}) \mu\text{b}, \tag{13}$$

where the first uncertainty is the sum in quadrature of the statistical and p_T dependent systematic uncertainty, and the second uncertainty is the fully correlated systematic uncertainty.

VII. SUMMARY

The exclusive decay $B^{\pm} \to J/\psi K^{\pm}$ has been used to measure the production cross section of the B^+ meson from data collected by the CDF detector. A sample size of 387 ± 32 events is obtained from $\int \mathcal{L} dt = 98 \pm 4$ pb^{-1} of 1.8 TeV $p\bar{p}$ collisions produced by the Fermilab Tevatron collider.

The measured total B^+ production cross section for $p_T(B) > 6.0$ GeV/c and $|y| < 1.0$ is

$$\sigma_B(p_T > 6.0 \text{ GeV}/c, |y| < 1.0) = 3.6 \pm 0.6(\text{stat} \oplus \text{syst}) \ \mu\text{b} \tag{14}$$

where the uncertainty is the sum in quadrature of the statistical and both correlated and p_T dependent systematic uncertainties. The differential cross section is measured to be $2.9 \pm 0.2 \ (\text{stat} \oplus \text{syst}_{p_T}) \pm 0.4 \ (\text{syst}_{fc})$ times higher than the NLO QCD predictions with agreement in shape. The first uncertainty is the sum in quadrature of the statistical and p_T dependent systematic uncertainty and the second is the correlated systematic uncertainty. The new measurement of the B^+ differential cross section confirms that the absolute rate is larger than the limits of that predicted by typical variations in the theoretical parameters.

These measurements supersede those of Ref. [6].

ACKNOWLEDGMENTS

We thank the Fermilab staff and the technical staffs of the participating institutions for their vital contributions. This work was supported by the U.S. Department of Energy and National Science Foundation; the Italian Istituto Nazionale di Fisica Nucleare; the Ministry of Education, Science, Sports and Culture of Japan; the Natural Sciences and Engineering Research Council of Canada; the National Science Council of the Republic of China; the Swiss National Science Foundation; the A.P. Sloan Foundation; the Bundesministerium fuer Bildung und Forschung, Germany; and the Korea Science and Engineering Foundation.

[1] P. Nason *et al.*, Nucl. Phys. **B327**, 49 (1989); **B335**, 260(E) (1990); W. Beeneker *et al.*, *ibid.* **B351**, 505 (1991).
[2] S. Frixione, M. Mangano, P. Nason, and G. Ridolfi, *Heavy Flavors II*, edited by A.J. Buras and M. Lindner, Advanced Series on Direction in High Energy Physics (World Scientific, Singapore, 1997).
[3] UA1 Collaboration, C. Albajar *et al.*, Phys. Lett. B **186**, 237 (1987); **256**, 121 (1991).
[4] CDF Collaboration, F. Abe *et al.*, Phys. Rev. Lett. **71**, 500 (1993); **79**, 572 (1997); **75**, 1451 (1995); D0 Collaboration, B. Abbott *et al.*, Phys. Lett. B **487**, 264 (2000); Phys. Rev. Lett. **85**, 5068 (2000).
[5] E.L. Berger, B.W. Harris, D.E. Kaplan, Z. Sullivan, T.M.P. Tait, and C.E.M. Wagner, Phys. Rev. D **63**, 115001 (2001).
[6] CDF Collaboration, F. Abe *et al.*, Phys. Rev. Lett. **75**, 1451 (1995).
[7] M.S. Alam *et al.*, Phys. Rev. D **50**, 43 (1994).
[8] CDF Collaboration, F. Abe *et al.*, Nucl. Instrum. Methods Phys. Res. A **271**, 388 (1988).
[9] S. Tkaczyk *et al.*, Nucl. Instrum. Methods Phys. Res. A **342**, 240 (1994); D. Amidei *et al.*, *ibid.* **360**, 137 (1995).
[10] D. Amidei *et al.*, Nucl. Instrum. Methods Phys. Res. A **350**, 73 (1994).
[11] G. Foster *et al.*, Nucl. Instrum. Methods Phys. Res. A **269**, 93 (1988).
[12] Particle Data Group, C. Caso *et al.*, Eur. Phys. J. C **3**, 1 (1998).
[13] CDF Collaboration, F. Abe *et al.*, Phys. Rev. D **57**, 5382 (1998); **59**, 032004 (1999); **58**, 092002 (1998).
[14] A. Martin, W. Stirling, and R. Roberts, Phys. Lett. B **306**, 145 (1993); **443**, 301 (1998); Eur. Phys. J. C **4**, 463 (1998).
[15] C. Peterson *et al.*, Phys. Rev. D **27**, 105 (1983).
[16] J. Chrin, Z. Phys. C **36**, 163 (1987).
[17] OPAL Collaboration, G. Alexander *et al.*, Phys. Lett. B **364**, 93 (1995); SLD Collaboration, K. Abe *et al.*, Phys. Rev. Lett. **84**, 4300 (2000); ALEPH Collaboration, A. Heister *et al.*, Phys. Lett. B **512**, 30 (2001).
[18] P. Avery, K. Read, and G. Trahern, ''QQ: A Monte Carlo Generator,'' CLEO Internal Software Note CSN-212, Cornell University, 1985.
[19] CDF Collaboration, F. Abe *et al.*, Phys. Rev. Lett. **75**, 4358 (1995).
[20] T. Keaffaber, Ph.D. dissertation, Purdue University, 2000.
[21] CDF Collaboration, F. Abe *et al.*, Phys. Rev. D **57**, R3811 (1998).
[22] CDF Collaboration, T. Affolder *et al.*, Phys. Rev. D **60**, 092005 (1999); Phys. Rev. Lett. **84**, 1663 (2000).
[23] CTEQ Collaboration, H.L. Lai *et al.*, Eur. Phys. J. C **12**, 375 (2000).